Effects of organic silicone additive material on physical and mechanical properties of mudstone

Zhaoyun Chai [*1,2], Tianhe Kang [1] and Weiyi Chen [2]

[1] *Mining Technology Institute, Taiyuan University of Technology, Taiyuan, Shanxi 030024, China*
[2] *Institute of Applied Mechanics and Biomedical Engineering, Taiyuan University of Technology, Taiyuan, Shanxi 030024, China*

Abstract. Mudstone is a very common rock that, when in contact with water, can exhibit considerable volume change and breakdown. This behavior of mudstone is frequently encountered in geotechnical engineering and has a considerable influence on infrastructure stability. This is particularly important in the present work, which focuses on mitigating the harmful properties of mudstone. The samples studied are of Permian Age mudstone from Shandong Province, China. Modification tests using organic silicone additive material were carried out. The mechanisms of physical properties modification of mudstone were comparatively studied using corresponding test methods, and the modification mechanism of organic silicone additive material acting on mudstone was analyzed. The following conclusions were drawn. The surface texture and characters of mudstone changed dramatically, surface character turns from hydrophilic to hydrophobic after organic silicone additive material modification. The changes in the surface character indicate a reduction in the water sensitivity of mudstone. After modification, the shape of porosity and fracture of mudstone changed unremarkable, and the total and free expansion ratios decreased obviously, whereas the strength increased markedly.

Keywords: mudstone; modified mechanism; swelling and shrinkage; microstructure; strength characteristics; long-term stability

1. Introduction

Mudstone and shale, which contain a large proportion of clay minerals, account for 50% of near-surface rock. Human engineering activities are often affected by the presence of mudstone in fields such as mining engineering, geotechnical engineering, hydraulic power engineering, tunneling, and underground storage. For a long time, the physical and mechanical properties of mudstone, such as swelling, reduced strength, and softening or disintegration (Dhakal *et al.* 2002, Doostmohammadi *et al.* 2008, Erguler and Ulusay 2009, Pejon and Zuquette 2002), have had huge effects on the stability of engineering construction (Jeng *et al.* 2002, Alejano *et al.* 2009, Corkum and Martin 2007, Shao *et al.* 2005, Erguler and Ulusay 2009, Pham *et al.* 2007, Hideo 2004). Mudstone, especially when it contains a significant clay fraction, is often weak rock and has motivated many studies (Dai *et al.* 2004, Jiang *et al.* 2001, Cai *et al.* 2004, Hart 1993). However, all existing theories and methods of controlling the stability of weak rock during engineering

---

∗Corresponding author, Ph.D., E-mail: chaizhaoyun_2002@163.com

projects have focused on passive support and anchorage, which involve changing the external factors of the weak rock. However, these strategies have substantial limitations and time requirements. Research has recently been undertaken to address the long-term stability of weak rock in an engineering project context by improving the physical and mechanical properties of the rock, this research is presently in an experimental investigation phase.

The literature (Chai *et al.* 2009, 2010) offers a proposal to prevent and delay the deterioration of weak-rock engineering properties by surface coating modifications. These researchers implemented and tested a system under indoor conditions and applied the results to engineering practice, which has achieved good social and economic benefits. However, this method does not change fundamentally the mechanical, physical, and chemical properties of the weak rock. A practical engineering example, the + 435 level mudstone roadway of the Liyazhuang coal mine (in the province of Shanxi, China), has shown that after only five to eight months, bottom caving made it necessary to enlarge the roadway to keep production running smoothly, grouting-coated reinforcement could extend production for two to three years beyond that, but could not ensure the long-term stability of the weak-rock roadway. To this end, in this research, the concept of using physical and chemical methods to change the material composition and microstructure of the weak rock have been expanded to effect fundamental changes in the physical and mechanical characteristics of the weak rock, with the objective of realizing long-term stability in weak-rock engineering. This research used silicone GJ657 as the additive material. The mechanism of changes in surface hydrophobic properties, porosity and fracture, swelling and shrinkage, microstructure, and physical and mechanical properties of mudstone were comparatively researched using the static water contact angle method, the nitrogen adsorption isotherm method, the free expansion test, SEM-EDS analysis, and the conventional rock mechanics strength test respectively, and the strengthening mechanism of organic silicone additive material modified mudstone were explored.

2. Experimental specimen and additive material

2.1 Experimental specimen

The specimen, which was taken from the floor of No. 1 coal seam in the Wali coal mine (in the province of Shandong, China), consisted of a lacustrine facies clastic sedimentary rock from the Cenozoic Paleogene Lijiaya formation. The specimen showed obvious laminar structure, exchangeable positive ions were K, Na, Ca, and Mg, the capacity was 42.5 meq/kg, the bulk density was 2500 kg/m^3, and the water content was 23.54%. An example of the X-ray diffraction patterns of the sample is shown in Fig. 1. The mineralogical composition of the sample was analyzed quantitatively using an adiabatic method. The contents of smectite, illite, chlorite, quartz, anorthose, calcite, pyrite, and dolomite in the sample were 20%, 10%, 10%, 40%, 10%, 5%, 3%, and 2% respectively. It is obvious that the main clay constituents were smectite, illite, and chlorite.

2.2 Additive material

The additive material, organic silicone GJ657, was obtained from Dow Corning Corporation, United States. This material is a natural infiltration stone protective agent and has strong chemosmotic properties, and it can repair fine fissures in rock samples.
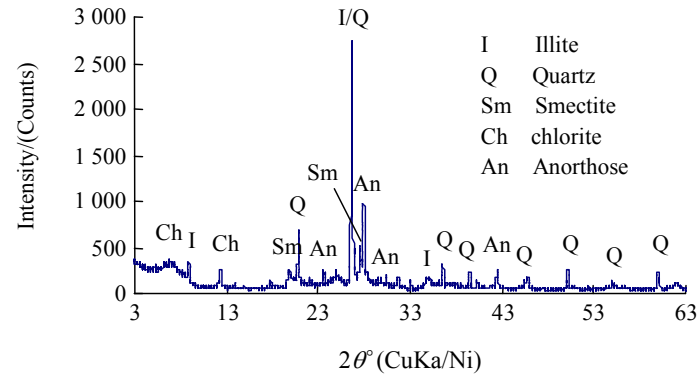
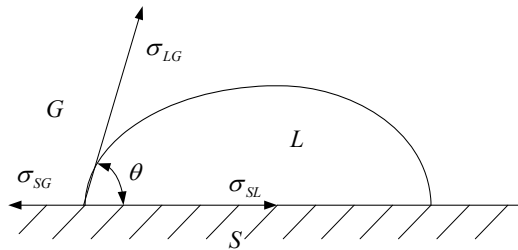Fig. 1 Representative X-ray diffraction pattern of a sample

Fig. 2 Diagram of triple contact among solid, liquid, and gas phases

3. Mechanisms of physical properties modification of mudstone

3.1 Surface hydrophobicity

Contact angle can be effectively used to characterize the surface hydrophobicity of materials. Among the many contact angle measuring methods, the static water contact angle method is commonly used. Its theoretical basis is to let the water drops in or on the surface of rock samples form a solid-liquid-gas three-phase interface, as shown in Fig. 2. When the three-phase interfacial tension is in equilibrium, it meets the Young equation (Young 1805)

$$\sigma_{SG} = \sigma_{SL} + \sigma_{LG} \cos\theta \tag{1}$$

where σ_{SG}, σ_{SL}, and σ_{LG} are the interfacial tension of the solid-gas, solid-liquid, and liquid-gas interfaces respectively, and θ is the static water contact angle. According to Eq. (1), the static water contact angle can be defined as follows: from the gas-liquid-solid three-phase contact point, drawn the tangent to the gas-liquid interface, and the angle between the tangent line and the liquid-solid interface is the static water contact angle. This angle varies from 0° to 180° depending on the shape of the droplets and the solid-surface hydrophobicity (the larger the value is, the stronger is the hydrophobicity, and conversely).

Static water contact-angle measurement procedures can be divided into two groups, unmodified and modified. In each, a group of five rock samples is taken; for each rock sample, two water droplets are measured, for a total of 10 measurements, and the average value is taken as the test value. The rock sample surface is a natural section in the direction of bedding plane rupture. The static water contact angle is measured using a contact-angle measuring instrument in an air environment at room temperature. Fig. 3 shows a photo of the water droplets on the rock sample surface, and the measurement results of the water-droplet contact angle on the rock sample surface are given in Table 1.

As can be seen from Fig. 3 and Table 1, the water droplets spread along the rock sample surface, and quickly penetrate inside rock sample for the unmodified, whereas the water droplet becomes spherical because of hydrophobic is enhanced for the modified, and water-contact angle increases from 8.51° to 113.34°. This clearly demonstrates that the organic silicone additive materials have changed the surface texture and characters of mudstone, and surface character turns from hydrophilic to hydrophobic.

3.2 Porosity and fracture

The experimental apparatus used was a Tristar3000 automatic physical adsorption instrument manufactured by Micrometrics Instrument Corporation, United States, using the principle of nitrogen adsorption. The experimental specimens were the same as those used for contact angle measurements. The specimens were ground into particles with a particle size less than 74 μm and kept under continuous vacuum for 12 h at 200 K before the test to remove volatile matter physically

(a) Unmodified   (b) Modified

Fig. 3 Photos of water drop on sample surfaces

Table 1 Measured results of contact angle of sample surfaces

Sample No.	Contact angle/(°)		Sample No.	Contact angle/(°)	
	Unmodified	Modified		Unmodified	Modified
1	Spread out	119.3	6	15.8	114.1
2	12.6	114.2	7	Spread out	113.7
3	Spread out	111.1	8	8.5	109.5
4	17.4	113.9	9	11.9	116.5
5	9.4	107.2	10	9.5	113.9

adsorbed on the samples. The test samples, in powder form in a natural stacked state, were then placed directly in a container to determine isothermal physical adsorption of nitrogen under liquid nitrogen cooling conditions. By measurement under different pressures of the amount of nitrogen gas adsorbed, the BJH method (Barrett *et al.* 1951) was used to characterize the pore structure and the main microstructural parameters of each sample. The density functional theory (Seaton *et al.* 1989) was used to calculate the full porosity distribution of each sample, and the standard BET method (Brunauer *et al.* 1938) to calculate the specific surface area of each sample.

Fig. 4 shows the nitrogen adsorption-desorption curve of the samples. It is apparent that: (1) when the relative pressure $P/P_0 < 0.8$, the amount of nitrogen adsorption in the samples slowly increased with increasing relative pressure. Along the starting portion of the adsorption curve, the adsorption occurred mainly in micropores, forming a thin layer only on the pore walls, which show that the samples have a single pore-size distribution; When the relative pressure $P/P_0 > 0.8$, the amount of nitrogen adsorption in the samples rapidly increased with further increases in relative pressure. This phenomenon may be explained if the samples contain a certain number of medium-sized and larger internal pores, which would lead to adsorption by capillary condensation;
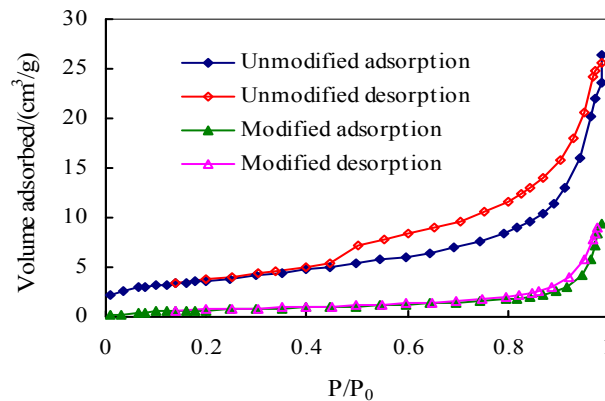

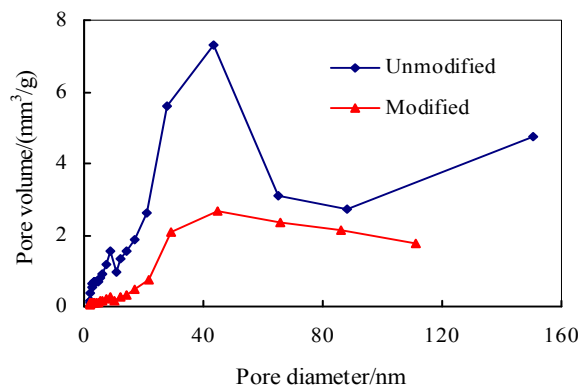Fig. 4 Low-temperature nitrogen isothermal adsorption-desorption curves of samples

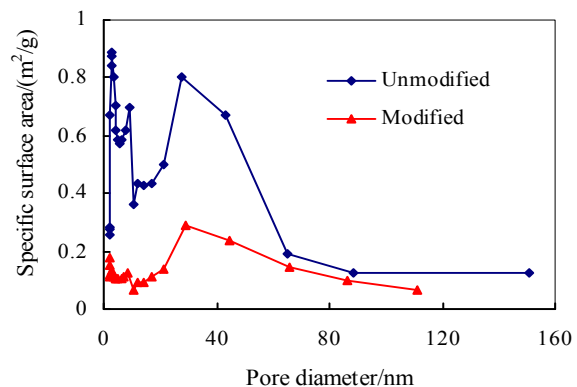Fig. 5 Relationship between pore diameter and pore volume of samples

Fig. 6 Relationship between pore diameter and specific surface area of samples

as more and more pores became filled, the adsorption and desorption branches would not overlap because of capillary condensation. A hysteresis loop would then appear, and the larger the loop, the greater would be the pore size. (2) The adsorption-desorption curve of the modified sample was significantly lower than that of the unmodified sample; the maximum amount of nitrogen adsorbed was 9.4773 cm^3/g, which was only 35.78% of the amount adsorbed by the unmodified sample, 26.4882 cm^3/g, and the BET-specific surface area was 2.8564 m^2/g, which was only 21.92% of the surface area of the unmodified sample, 13.0298 m^2/g.

Fig. 5 shows the relationship between the diameter of pore and the volume, and Fig. 6 shows the relationship between the diameter of pore and specific surface area. From these curves, it is clear that: (1) the diameter of pore in the samples was concentrated in the 2.8-nm, 9-nm, and 27.9-nm ranges. The 2.8-nm represents the lattice spacing of the clay minerals contained in the samples, the 9-nm represents the porosity of the clay mineral micro-aggregates, and the 27.9-nm represents the porosity of the sample skeleton particles. (2) The volume of pore was determined mainly by the sample skeleton particles. Among them, the diameter of pore is 43.4 nm approximately, and the volume was 7.288 mm^3/g, which was 17.5% of the total volume, 41.647 mm^3/g. (3) The pore morphology of the modified samples showed little change in distribution, but the total was significantly reduced by the role of the additive materials, the maximum pore diameter being reduced from approximately 150 nm (unmodified samples) to approximately 110 nm.

3.3 Swelling and shrinkage

Swelling and shrinkage characteristics were evaluated by comparing the free expansion ratios of modified and unmodified samples. A single specimen was processed into six cylindrical samples, each 50 mm in diameter and 25 mm in height, with the head surface parallel to the bedding plane. The first step was to put the rock samples into the expansion loop in the experiment, working carefully to ensure that the rock sample was set into the expansion loop and that friction between the samples and the loop was minimized during sample loading, and a thin layer of Vaseline was applied to the hoop of samples. Following which the expansion loop with the
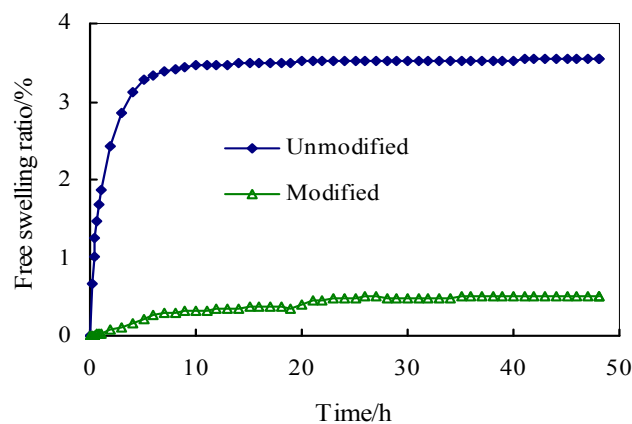

Fig. 7 Relationship between free expansion ratios of samples and time

samples was immersed in distilled water, with the liquid level 1 cm above the upper surface of the samples. To prevent debris from plugging holes during the immersion process, qualitative filter paper should be placed on the upper and lower surfaces of the samples. Any sample height changes were recorded by a displacement sensor which was placed in the center position on the surface of the sample. The experiment was carried out by dividing the samples into unmodified and modified groups, with three samples in each group, and taking the average value of the three samples as the test value. Fig. 7 shows the changes in the free expansion ratios of the samples with time.

It can be seen from Fig. 7 that: (1) the rock sample expansion curve is initially steep, then rises more slowly, and finally stabilizes, with expansion of the unmodified and modified samples reaching a steady state in approximately 10 and 20 hours respectively. This provides evidence for mudstone engineers that expansion of mudstone can be expected to continue for a long time, but that the majority of the expansion will be completed in a short time. Once the majority of the expansion has occurred, project construction can begin, without having to wait for the final steady state. (2) Stable free expansion of the modified sample was 0.51%, and only 14.4% of that of the unmodified sample, 3.54%. This phenomenon may have occurred because the additive material penetrated inside the sample, changing the expansion behavior of the crystalline structures contained in the clay mineral. Another reason could have been that the additive material entered the pores and fractures of the samples, sealing migrating moisture inside and outside the sample channel, and thereby changing the swelling and shrinkage behavior of the rock.

3.4 Microstructure and chemical composition

Microstructure and chemical composition were tested using a LEO1450VP scanning electron microscope manufactured by Leo Instrument Corporation, Germany. The test was carried out by dividing the samples into unmodified and modified groups, five samples in each group, taking four magnifications ($\times$ 80, $\times$ 400, $\times$ 2000, and $\times$ 4000) with SEM + EDS analysis for every sample, and taking the average value as a test value for the chemical element composition of the sample. A tungsten filament electron gun was used for the test, with a magnification of 100000 times, a resolution of 3 μm, and a vacuum pressure of 1–400 Pa. The sample was placed in the oven at low temperature (-50°C) to remove water, followed by vacuum spray plating, ensuring that the observation surface was a fresh, clean, and relatively flat natural fracture plane. Fig. 8 shows an SEM+EDS photo of one sample from the unmodified and modified groups, and Table 2 shows the EDS test results for chemical element composition of samples from the unmodified and modified groups.

As can be seen from Fig. 8, the unmodified sample contains a large quantity of clay minerals, locally visible curling sheet smectite, and a small sheet of clay mineral particles which enter into surface or edge-face contact with each other to form larger aggregates. Looking at the arrangement of the aggregates, the pore structure consists mainly of inter-granular and inter-aggregate pores, and most of the pore sizes range from a few tenths of a micron to a few microns, as shown in Fig. 8(a). The inter-granular pores of the clay minerals in the modified samples were filled by the additive material cemented to form larger aggregates. Because flaky clay minerals were not found, it could be concluded that the porosity was mainly inter-aggregate, that the pore shape was approximately isotropic, and that the number of pores was significantly less than in the unmodified samples, as shown in Fig. 8(b). As can be seen from Table 2, the proportions of chemical elements differed greatly between the modified and unmodified samples. The amount of carbon in the
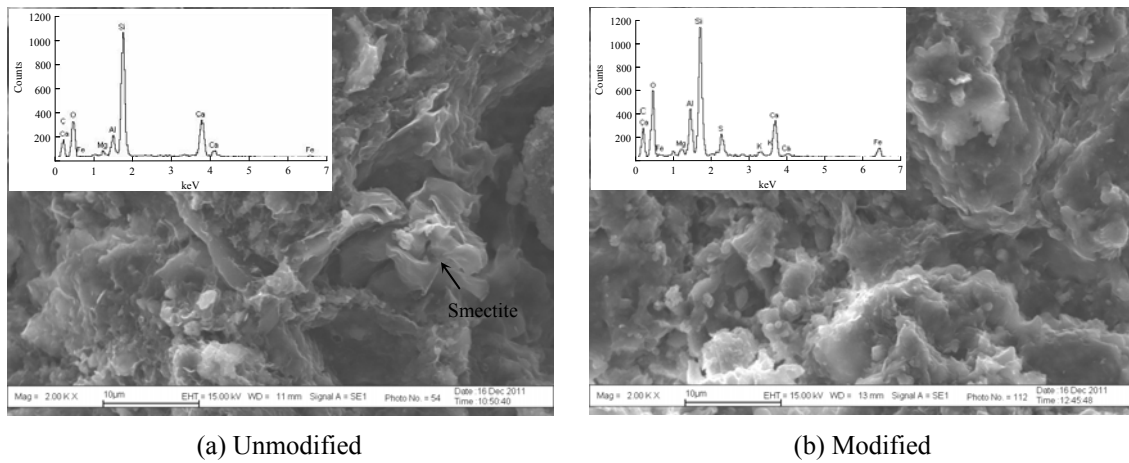
(a) Unmodified   (b) Modified

Fig. 8 SEM images and EDS spectra of samples

Table 2 EDS analysis results for elemental composition of samples

Samples	W/%									
	O	Na	Mg	Al	Si	S	K	Ca	Fe	C
Unmodified	49.68	0.08	0.54	2.04	16.11	-	0.31	13.42	0.59	17.19
Modified	45.73	0.08	0.62	2.26	10.01	1.00	0.17	5.51	1.38	33.09

modified samples had increased greatly, and sulfur was also found, which confirmed that additive materials had infiltrated the samples internally. On the one hand, these materials filled internal pores and fractures which were interconnected inside the samples, preventing moisture migration inside and outside the samples. While on the other hand, they cemented hydroxide radicals into the sample surfaces, which improved the matrix structure of the samples, further enhancing their mechanical strength.

3.5 Strength characteristics

Mechanical strength was tested using a JL-WAW60 PC-controlled electro-hydraulic servo universal testing machine manufactured by Jilin Test Technology (Changchun, China). The maximum load capacity of the frame was 6.0×10^4 kg, the minimum displacement rate was 1.0×10^{-3} mm/s, and the loading rates could be varied using the servo control system. Following ISRM suggested methods (ISRM 1979), uniaxial compression tests and Brazil tests were carried out by dividing the samples into unmodified and modified groups, with three samples in each group. The uniaxial compression test was performed on selected cylindrical samples 50 mm in diameter and 100 mm in height, with a displacement rate of 8×10^{-3} mm/s. The Brazil test was performed on selected disk samples 50 mm in diameter and 25 mm in height, with a displacement rate of 5×10^{-2} mm/s.

The complete stress-strain curves obtained from the samples are shown in Fig. 9. The results from mechanical strength testing of samples are listed in Table 3. It can be seen from Fig. 9 and
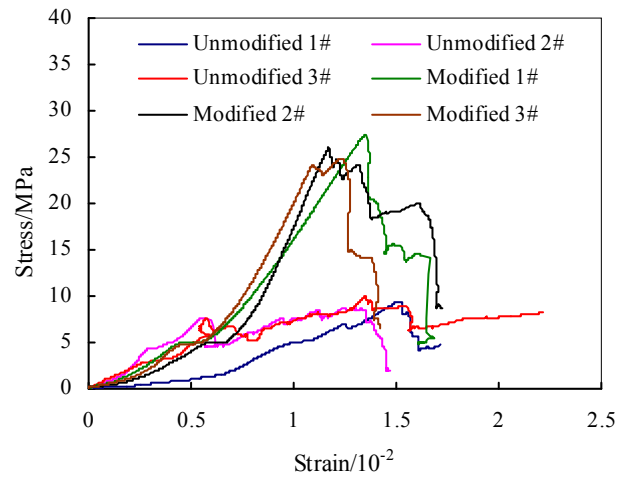
Fig. 9 Uniaxial compressive stress-strain curves of samples

Table 3 Test results for mechanical strength of samples

Test method	State	Sample No.	Size/mm	Failure loading/kN	Strength/MPa	Mean of strength/MPa
Uniaxial compression test	Unmodified	1	49.4 × 100.8	18.05	9.41	
		2	49.9 × 100.6	17.12	8.53	9.3
		3	49.6 × 100.6	19.25	9.96	
	Modified	1	49.7 × 99.3	53.17	27.38	
		2	49.6 × 101.2	50.18	25.99	26.05
		3	49.5 × 99.8	47.68	24.77	
Brazil test	Unmodified	1	49.4 × 25.8	3.32	1.73	
		2	49.6 × 25.4	2.88	1.49	1.69
		3	49.4 × 24.8	3.50	1.84	
	Modified	1	49.5 × 25.6	5.91	2.97	
		2	49.4 × 25.0	6.09	3.14	3.22
		3	49.3 × 24.9	6.83	3.54	

Table 3 that: (1) the mechanical strength of the modified samples was obviously enhanced. The mean uniaxial compression strength of the modified samples was 26.05 MPa, and 2.8 times that of the unmodified samples, 9.3 MPa, and the mean tensile strength of the modified samples was 3.22 MPa, and 1.9 times that of the unmodified samples, 1.69 MPa. (2) Stress in unmodified samples 2 and 3 decreased after peak stress values of 7.69 MPa and 7.64 MPa respectively. With further strain increase, these samples reached failure stresses and underwent repeated fluctuations. This occurred due to frictional resistance induced by slippage relative to the failure plane and generated along the fracture surface after sample failure. Failure of the samples transitioned gradually from brittle failure into ductile failure, with stress values closely related to the roughness of the failure

Table 4 E and E_d test results from mechanical strength testing of samples

State	Sample No.	Elastic modulus E /MPa	Deformation modulus E_d /MPa
Unmodified	1	692	621
	2	1254	681
	3	1062	678
Modified	1	3044	2034
	2	4990	2223
	3	3721	2014

plane and contact state of the sample particles (You and Su 2004). (3) If the tangent value (peak stress of 40%–60%) in the elastic region of the complete stress-strain curve is defined as the elastic modulus E, and the secant value between the peak intensity and the origin of the coordinate system is defined as the deformation modulus E_d. Table 4 shows the E and E_d test results from mechanical strength testing of modified and unmodified samples. It can be seen from Table 4 that the mean elastic moduli of the three samples in the unmodified and modified groups were 1002 MPa and 3918 MPa respectively, and the mean deformation moduli of the three samples in the unmodified and modified groups were 660 MPa and 2090 MPa respectively. Obviously, the modified samples exhibited higher values of both the elastic modulus and the deformation modulus than did the unmodified samples, these properties are conducive to the long-term stability of weak-rock engineering.

4. Organic silicone modification mechanism in mudstone

The organic silicone additive material is an organopolysiloxane compound with a molecular structure containing elemental silicon, a repeating Si-O bond as the main chain, and an organic group connected to the silicon atom. A polymerization reaction occurs when organic silicone contacts mudstone, in which the electric double layer of the clay and colloidal particle surface is destroyed, the surface structure and nature of the sample is changed, and hydrophobic mesh molecules form on the surface and capillary walls of the sample, as shown in Fig. 10. Consequently, the surface tension of the sample was reduced, the surface charge properties of the clay and the colloidal particles were improved, and electro-chemical bonds between the surface charge and the hydrone were broken. Furthermore, the water which had been bound in the adsorption layer and the diffusion layer was released, the thickness of the water film on the sample surface was reduced, the induced ζ potential was reduced, and the water contact angle of the samples was increased, preventing capillary pores from absorbing water. At the same time, the organic silicone material penetrated the inner, filled, and bound wall pores of the samples, so that the porosity of these samples was reduced, the bonding strength among the rock particles was enhanced, and the strength and deformation rate of the samples was increased. Meanwhile, the movement of water within the sample was restricted because of the hydrophobic properties of the siloxane, and the softening and disintegration properties of the mudstone were fundamentally changed.
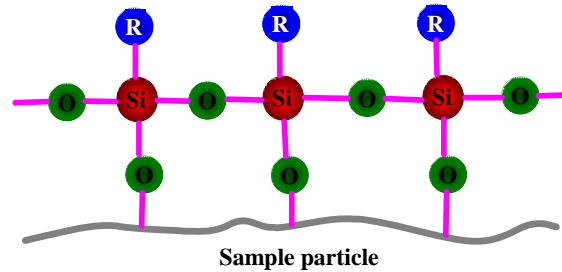
Fig. 10 Hydrophobic mechanism of organic silicone

5. Discussion

In practical engineering applications involving mudstone modified by grouting with organic silicone additive materials, the differences from traditional grouting methods are: (1) the object of grouting. The conventional object of grouting generally has been broken or softened weak rock in process of disintegration. In this research, the object of grouting has been weak rock in pristine condition. If porosity, fracture development, and inter-connectivity are good and can facilitate the penetration and diffusion of grout, then grouting is good. If the development and inter-connectivity of porosity and fractures is inferior, then grouting is poor. (2) Grout and its characteristics vary. The traditional grouting approach was to use Portland cement grouting, with which the strength of the stone body was higher, costs were lower, raw material sources were more widespread, and grout preparation was more convenient. However, Portland cement grouting can generally be injected only into pores or fractures of diameter or width greater than 0.2 mm because of particle size. On the other hand, modified organic silicone grouting, which has low viscosity and high permeability, can be injected into pores or fractures of diameter or width greater than a few micrometers to a few tenths of a micrometer. (3) The properties and rules of grout flow in the geotechnical layer are different. The flow of grouting cement within the rock and soil mass, which is driven mainly by grouting stress, water separation, and precipitation, is more severely restricted, the diameter of penetration and diffusion will be smaller. When grouting with modified organic silicone within a rock and soil mass, the flow is driven not only by grouting stress, but also by chemical bond forces between hydroxyl ions on the surfaces of the sample and the grout. These create a tendency to spontaneous infiltration and can lead to penetration of fine pores without water precipitation.

6. Conclusions

(1) Modification of mudstone by organic silicone additive material not only effectively changes the sample surface structure and properties and converts the rock surface from hydrophilic to hydrophobic, but also penetrates inside the sample and changes its internal matrix structure, reducing its propensity to swelling and shrinkage.

(2) The strength of the modified samples was significantly increased. The uniaxial compressive strength of the modified samples was increased to 2.8 times that of the unmodified samples, and the tensile strength of the modified samples was increased to 1.9

times that of the unmodified samples. Compression failure of the unmodified samples occurred after the loading exceeded their intrinsic strength because of plastic slippage due to friction between failure planes. In other words, the failure transitioned from brittle failure to ductile failure. The stress of the modified sample rapidly decreased after reaching peak loading, obviously due to brittle failure.

These conclusions have been drawn based on indoor small-sample tests. How to apply these conclusions to the scale of rock mass addressed in engineering and how to use them effectively are matters which remain real concerns for engineering and technical staff. A systematic study would need to take into account the difference between engineering rock mass and small sample size, modifications in technology as applied to engineering practice, geological storage conditions, the chemical composition, porosity, and fracture extent of the engineering rock mass, and the permeability of the materials used for modification.

Acknowledgments

References

Alejano, L.R., Rodriguez-Dono, A., Alonso, E. and Fdez-Manin, G. (2009), "Ground reaction curves for tunnels excavated in different quality rock masses showing several types of post-failure behaviour", *Tunn. Undergr. Sp. Tech*., **24**(6), 689-705.

Barrett, E.P., Joyner, L.G. and Halenda, P.P. (1951), "The determineation of pore volume and area distribution in porous substances. I Computing from nitrogen isotherms", *J. Am. Chem. Soc*., **73**(1), 373-380.

Brunauer, B.S., Emmett, P.H. and Teller, E. (1938), "Adsorption of gases in multi-molecular layers", *J. Am. Chem. Soc*., **60**(1), 309-319.

Cai, Y., Esaki, T. and Jiang, Y. (2004), "An analytical model to predict axial load in grouted rock bolt for soft rock tunneling", *Tunn. Undergr. Sp. Tech*., **19**(6), 607-618.

Chai, Z., Kang, T. and Yang, Y. (2009), "Evaluation of silicon modified resin for coated soft rock with high montmorillonite content and its effects", *Chinese J. Rock Mech. Eng*., **28**(1), 81-87.

Chai, Z., Kang, T. and Yang, Y. (2010), "Experimental study on coated modification of soft rock with high kaolinite content", *J. China Coal Soc*., **35**(5), 734-738.

Corkum, A.G. and Martin, C.D. (2007), "The mechanical behaviour of weak mudstone (Opalinus Clay) at low stresses", *Int. J. Rock Mech. Min. Sci*., **44**(2), 196-209.

Dai, H.L., Wang, X., Xie, G.X. and Wang, X.Y. (2004), "Theoretical model and solution for the rheological problem of anchor-grouting a soft rock tunnel", *Int. J. Pressure Vessels Piping*, **81**(9), 739-748.

Dhakal, G., Yoneda, T., Kato, M. and Kaneko, K. (2002), "Slake durability and mineralogical properties of some pyroclastic and sedimentary rocks", *Eng. Geol*., **65**(1), 31-45.

Doostmohammadi, R., Moosavi, M. and Araabi, B.N. (2008), "A model for determining the cyclic swell-shrink behavior of argillaceous rock", *Apply Clay Sci*., **42**(1/2), 81-89.

Erguler, Z.A. and Ulusay, R. (2009), "Water-induced variations in mechanical properties of clay-bearing rocks", *Int. J. Rock Mech. Min. Sci*., **46**(2), 355-370.

Hart, P.A. (1993), "Foundation behaviour in reusable tunnels in weak rocks", *Int. J. Rock Mech. Min. Sci. Geomech. Abstr.*, **30**(3), 239-246.

Hideo, K. (2004), "Simplified evaluation for swelling characteristics of Bentonites", *Eng. Geol.*, **71**(3/4), 265-279.

ISRM (1979), Suggested methods for determining the uniaxial compressive strength and deformability of rock materials.

Jeng, F.S., Wang, M.C., Huang, T.H. and Liu, M.L. (2002), "Deformational characteristics of weak sandstone and impact to tunnel deformation", *Tunn. Undergr. Sp. Tech.*, **17**(3), 263-274.

Jiang, Y., Yoneda, H. and Tanabashi, Y. (2001), "Theoretical estimation of loosening pressure on tunnels in soft rock", *Tunn. Undergr. Sp. Tech.*, **1**(2), 99-105.

Pham, Q.T., Vales, F., Malinsky, L., Minh, D.N. and Gharbi, H. (2007), "Effects of desaturation resaturation on mudstone", *Phys. Chem. Earth, Parts A/B/C*, **32**(8-14), 646-655.

Pejon, O.J. and Zuquette, L.V. (2002), "Analysis of cyclic swelling of mudrocks", *Eng. Geol.*, **67**(1/2), 97-108.

Seaton, N.A., Walton, J.P. and Quirke, N. (1989), "A new analysis method for the determination of the pore size distribution of porous carbons from nitrogen adsorption measurements", *Carbon*, **27**(6), 853-861.

Shao, J.F., Ata, N. and Ozanam, O. (2005), "Study of desaturation and resaturation in brittle rock with anisotropic damage", *Eng. Geol.*, **81**(3), 341-352.

You, M. and Su, C. (2004), "Effect of length of fine and coarse crystal marblespecimens on uniaxial compression tests", *Chinese J. Rock Mech. Eng.*, **23**(22), 3754-3760.

Young, T. (1805), "An essay on the cohesion of fluids", *Philosophical Transactions of the Royal Society of London*, **95**(1), 65-87.

PL